Available online at www.sciencedirect.com
ScienceDirect
Journal of Energy Chemistry 23(2014)391–396
JOURNAL OF ENERGY CHEMISTRY
www.elsevier.com/journals/journal-of-energy-chemistry/2095-4956
www.elsevier.com/locate/jngc

Sulfur/carbon composites prepared with ordered porous carbon for Li-S battery cathode

Xin Zhuang, Yingjia Liu, Jian Chen*, Hao Chen, Baolian Yi

Lab of Advanced Rechargeable Batteries, Dalian Institute of Chemical Physics, Chinese Academy of Science, Dalian 116023, Liaoning, China

[Manuscript received December 23, 2013; revised March 24, 2014]

Abstract

Ordered porous cabon with a 2-D hexagonal structure, high specific surface area and large pore volume was synthesized through a two-step heating method using tri-block copolymer as template and phenolic resin as carbon precursor. The results indicated the electrochemical performance of the sulfur/carbon composites prepared with the ordered porous carbon was significantly affected by the pore structure of the carbon. Both the specific capacity and cycling stability of the sulfur/carbon composites were improved using the bimodal micro/meso-porous carbon frameworks with high surface area. Its initial discharge capacity can be as high as 1200 mAh·g^{-1} at a current density of 167.5 mA·g^{-1}. The improved capacity retention was obtained during the cell cycling as well.

Key words

lithium-sulfur battery; sulfur/carbon composite; ordered porous carbon; bimodal micro/meso-porous carbon; tri-block copolymer

1. Introduction

The low energy density in the rechargeable batteries has become one of the limitations for the further applications in advanced electrical vehicles (EVs) and portable electronic devices. Sulfur with an extremely high theoretical specific capacity of 1672 mAh·g^{-1} has been considered as a promising cathode candidate. The theoretical specific energy for the Li-S battery can reach 2600 Wh·kg^{-1} [1]. However, due to the poor electrochemical property and cycle stability of sulfur electrode, the Li-S batteries still suffer from several challenges for its practical application. First, sulfur is an electronic and ionic insulator. Second, lithium polysulfides (Li_2S_x, $4 \leq x \leqslant 8$), the intermediate discharge products are soluble in the organic electrolyte. Their shuttle effect between the cathode and anode could lead to sulfur mass loss, current leakage, charge/discharge efficiency decay, and thus cell performance degradation. Besides, the insoluble and insulated final product Li_2S can block the pathway for ions and electrons transportation and cause cathode failure. Many efforts have been conducted to solve these problems, and utilizing the sulfur/carbon (S/C) composites has been demonstrated as an effective approach to improve the electrochemical property of sulfur cathode [2]. Various porous carbon materials have been investigated for the sulfur/carbon composites, e.g. carbon blacks [3], mesoporous carbons [4], carbon nanotubes(CNTs) [5], and carbon fibers [6]. Their pore structure and surface property have shown to favor the electrical conduction and improve the capacity and the cycling stability [7]. Liang et al. [8] synthesized a hierarchically structured S/C nanocomposite with a high initial discharge capacity of 1584 mAh·g^{-1} at a current density of 2.5 A·g^{-1} in LiTFSI/(DOL+DME) electrolyte. Chen et al. [4] also reported an ordered mesoporous carbon/sulfur nanocomposites prepared via heat treatment, which delivered a high initial discharge capacity of 1138 mAh·g^{-1} at 0.1 C rate. It exhibited excellent stability with a capacity of 274 mAh·g^{-1} even after 400 cycles at ~6 C (7 A·g^{-1}) rate.

Herein, the mesoporous carbons with different pore-size distribution were successfully synthesized for the S/C composite cathode. The effects of the mesopore structure in the carbon frameworks on the electrochemical properties and cycling performance of the composite were also investigated.

2. Experimental

2.1. Preparation of ordered porous carbon

Two kinds of ordered porous carbon, named as MC-1 and

* Corresponding author. Tel: +86-411-84379687; Fax: +86-411-84379687; E-mail: chenjian@dicp.ac.cn

This work was supported by the National High Technology Research and Development Program of China (863 Program) and the Strategic Priority Research Program of the Chinese Academy of Sciences.

doi: 10.1016/S2095-4956(14)60162-5

MC-2, were synthesized, respectively. Their procedures are in the following.

The MC-1 was prepared following the method reported by Meng et al. [8]. 1.0 g tri-block copolymer F127 (Sigma) was dissolved in 20.0 g ethanol under stirring. 5.0 g 20 wt% resol precursors in ethanol solution was added. The resol was prepared using a polymerization method driving from phenol and formaldehyde reported elsewhere [9]. A homogeneous solution was obtained after further stirring for 10 min, which was then transferred into petri dishes and dried at room temperature for 5−8 h with an additional heat treatment at 100 °C for 24 h in an oven. The resultant transparent orange films were collected and ground into powders, and finally calcinated at 900 °C in an Ar atmosphere to generate MC-1.

1.0 g the as-prepared MC-1 was mixed with 4.0 g KOH solids. The mixtures were heated at 850 °C for 2 h in a tube furnace in an Ar atmosphere. The sample was first washed with copious HCl solution to remove KOH and then washed with de-ionized water to neutral. The final MC-1 treated by KOH named as MC-1-KOH was obtained after drying.

MC-2 was synthesized according to Liu et al. report [10]. 1.0 g F127 was dissolved in 8 g ethanol with 1 mL 0.2 mol/L HCl solution at 40 °C under stirring for 1 h. 2.08 g TEOS and 5.0 g 20 wt% resol in ethanol solution were then added into the clear solution and stirred for 2 h. The following procedures of drying and calcination were the same as the above description for the preparation of MC-1. The products, carbon-silica composites were immersed in 10% HF in ethanol solutions for 24 h to remove the silicas. Further washing and drying were conducted to obtain MC-2.

2.2. Preparation of sulfur/carbon composites

The as-prepared porous carbon materials (i.e. MC-1, MC-1-KOH, and MC-2) were mixed with the elemental sulfur (99.5%, Tianjin Damao Chemical Corp.) with a weight ratio of 1 : 5 in a planetary mill for 5 h, respectively. After then, the mixtures were heated at 150 °C for 15 h and then at 300 °C for 1 h, and cooled down to room temperature to yield the final S/C composites. Since the above mentioned heat treatment will not cause mass loss in the porous carbon, the sulfur content in the composites can be calculated based on their mass change. Thus, the corresponding sulfur contents in the S/MC-1, S/MC-1-KOH, and S/MC-2 composites are 39.8%, 37.5%, and 58.7%, respectively.

2.3. Assembly of Li-S cells

The sulfur cathodes were prepared by mixing S/C composites, acetylene black and polyvinylidene fluoride (PVDF) with a weight ratio of 7 : 2 : 1 in the ethanol to prepare a viscous homogeneous paste. The paste was then pressed into an electrode film with thickness of $\sim$100 μm using a twin-rollers machine. The as-prepared electrode membrane was dried at 50 °C for 12 h in a vacuum. Then, it was cut into square sheets with the dimension of 1 cm$\times$1 cm to be served as the cathodes. Then the sulfur electrodes were dried at 58 °C under vacuum for 24 h before use.

The CR 2016-type coin cells were assembled in an argon-filled glove box using the composite cathode and lithium metal anode. A 1 mol/L of LiTFSI in the DME/DOL (1 : 1, v/v) solution was used as the electrolyte with a Celgard 2400 membrane as the separator.

2.4. Characterizations

The crystal structures of the synthesized porous carbons and their corresponding S/C composites were characterized using an X'pert Pro X-ray diffractometer (XRD, PANalytical, The Netherlands). The nitrogen adsorption isotherms of specimens were tested at 77 K using a QuadraSorb SI 4 physisorption analyzer (Quantachrome Instruments, USA).

The charge/discharge performances were tested at a current density of 165 $mA\cdot g^{-1}$ in the voltage range between 1.5 V and 3.0 V using a CT2001A battery tester (LAND, Wuhan, China) at room temperature.

3. Results and discussion

3.1. Structure of the porous carbons

Figure 1 shows the small-angle XRD patterns of the as-prepared porous carbons: (a) MC-1, (b) MC-1-KOH, and (c) MC-2, respectively. Two peaks that can be indexed as (100) and (110) were observed for the three materials, indicating that the carbon materials have an ordered 2-D hexagonal structure with the space group P6mm [11].

The nitrogen adsorption isotherms of the three carbons and the corresponding pore-size distributions are shown in Figure 2. As for MC-1-KOH and MC-2, the nitrogen adsorption isotherms can be catalogued as Type IV curves which suggest a mesoporous carbon structure [12]. The physicochemical properties of the ordered porous carbons MC-1, MC-1-KOH, and MC-2 are listed in Table 1. The specific surface areas are 611, 1387 and 2137 $m^2\cdot g^{-1}$ with the corresponding pore volumes of 0.34, 0.81 and 1.8 $cm^3\cdot g^{-1}$, respectively. The analysis from nitrogen adsorption indicated that the surface area (482 $m^2\cdot g^{-1}$) and pore volume (0.25 $cm^3\cdot g^{-1}$) of MC-1 were attributed to the micropores with pore size of 1.6 nm [13]. The surface area and pore volume of the mesopores in MC-1-KOH are 980 $m^2\cdot g^{-1}$ and 0.51 $cm^3\cdot g^{-1}$, respectively. The KOH activation in MC-1 was demonstrated to contribute to the generation of mesopores with pore size of 2.9 nm [14]. Compared with the other two porous carbons, MC-2 exhibited higher surface area, larger pore volume and also a bimodal micro/mesoporous structure with pore sizes averaged at 1.9 nm and 6.5 nm. The 10% HF was found to have little effect on the primary mesoporous structure in MC-2. The unique physicochemical properties of MC-2 can be ascribed to its interconnected secondary pore channels which were generated from the removal of silicon species in the carbon framework [10]. Scheme 1 illustrates the detailed schemes of the ordered porous carbons (a) MC-1 and (b) MC-2, which clearly reflects their difference in the porous structure.

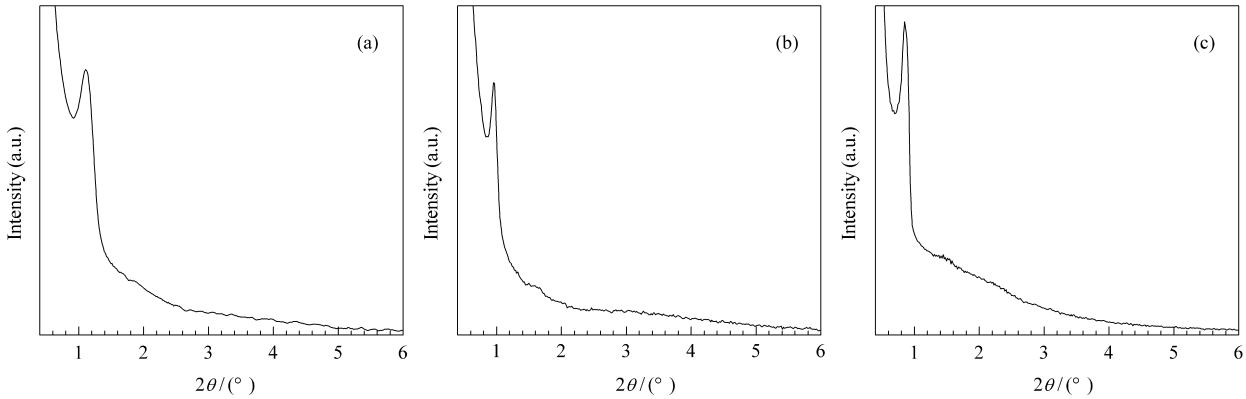

Figure 1. Small-angle XRD patterns of ordered porous carbons: (a) MC-1, (b) MC-1-KOH, and (c) MC-2

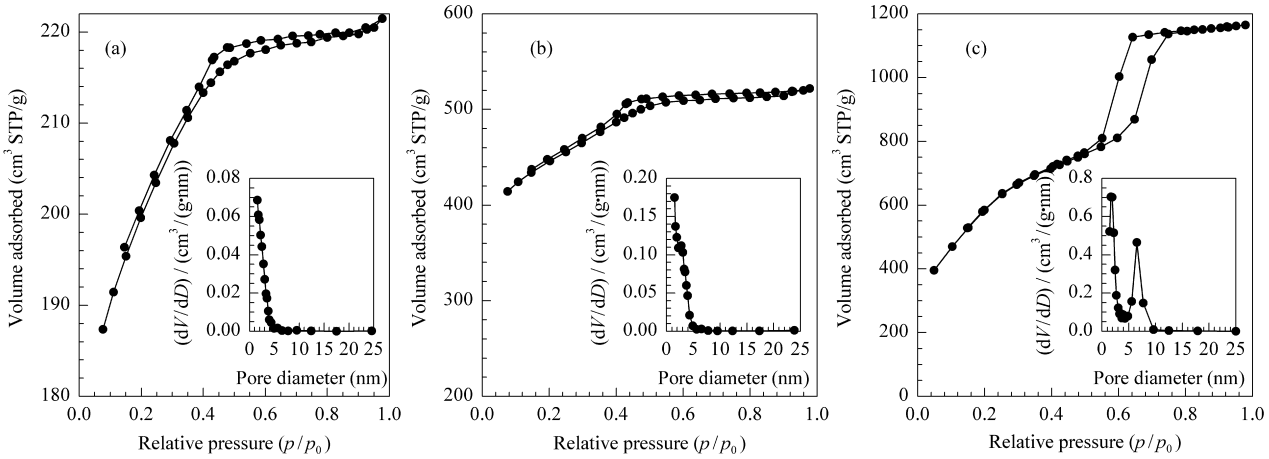

Figure 2. Nitrogen adsorption/desorption isotherms of ordered porous carbons: (a) MC-1, (b) MC-1-KOH, and (c) MC-2 with inset showing the corresponding pore-size distributions

Table 1. Physicochemical properties of the porous carbons before and after encapsulating sulfur

Samples	S_{BET} ($m^2 \cdot g^{-1}$)	S_{BET}^{micro} ($m^2 \cdot g^{-1}$)	V^{total} ($cm^3 \cdot g^{-1}$)	V^{micro} ($cm^3 \cdot g^{-1}$)	D (nm)
MC-1	611	482	0.34	0.25	1.6
S/MC-1	12	0	0.04	0.00	–
MC-1-KOH	1387	980	0.81	0.51	2.9
S/MC-1-KOH	148	0	0.12	0.00	2.9
MC-2	2137	0	1.80	0.00	1.9/6.5
S/MC-2	397	0	0.48	0.00	1.9/6.5

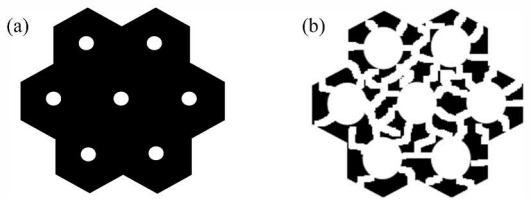

Scheme 1. Schematic illustrations of the ordered porous carbons (a) MC-1 and (b) MC-2

3.2. Structure of the sulfur/carbon composites

Figure 3 shows the wide-angle XRD patterns of the pure sulfur, as-prepared ordered porous carbons and S/C composites, respectively. The multiply intense peaks with the strongest one at $2\theta = 21.5^{o}$ suggested an excellent crystallinity of sulfur. All the porous carbons exhibited broad reflections at 22^{o} and 44^{o} indicating the formation of a graphitic-type structure with limited crystallization in the MC-1, MC-1-KOH, and MC-2. The S/MC-1 composite had similar XRD patterns to the sulfur, which could be due to the sulfur aggregation on the carbon surface caused by the small pore size of MC-1 that retarded sulfur encapsulation. However, the characteristic sulfur peaks were not easily observed in the XRD patterns of S/MC-1-KOH and S/MC-2. The results suggested that most sulfur had been well distributed into the mesopores in the framework of the carbons to form the amorphous phase in S/MC-1-KOH and S/MC-2 [15].

Figure 4 displays the nitrogen adsorption isotherms of the S/C composites, (a) S/MC-1, (b) S/MC-1-KOH, and (c) S/MC-2, respectively. Their specific surface areas are calculated to be 12, 148 and 397 $m^2 \cdot g^{-1}$ with the pore volumes of 0.04, 0.12 and 0.48 $cm^3 \cdot g^{-1}$, respectively. The reduction in the surface area and pore volume in the S/C composites confirms that sulfur had occupied the majority of the pores in the carbon matrixes for the three samples. Multiply hysteresis loops in Figure 4(a) implies that S/MC-1 had a wide pore-size

distribution (also shown in inset), which could be related to the partial encapsulation of sulfur in the micropores in MC-1 and the piled pores caused by the aggregation of sulfur on the carbon surface. As shown in Figure 4(b), S/MC-1-KOH possessed the typical Type IV isotherm but with an unclosed hysteresis loop which may be resulted from the adsorption of sulfur. The pore size of S/MC-1-KOH (inset in Figure 4b) was comparable to that of MC-1-KOH (inset in Figure 2b). The obvious reduction of the volume and surface area of the micropores in S/MC-1-KOH indicates the encapsulation of sulfur within the small meso-pores in MC-1-KOH carbon. The typical Type IV curve of S/MC-2 as shown in Figure 4(c) reveals a bimodal pore-size distribution close to that of MC-2. The obvious reduction of the pore volume of the micropores with pore size of 1.9 nm suggests that most of the sulfur were embedded in the micropores. The results obtained from BET analysis indicate that the different sulfur distributions in the three composites depend on the porous structure of the carbon framework, which also agrees well with the XRD results. The smaller pore size in MC-1 depressed the adsorption of molten sulfur, whereas the larger mesopores in MC-1-KOH favored the sulfur encapsulation. As for MC-2, its unique bimodal micro/mesoporous structure is more benefit to providing larger pore volume and surface area for higher sulfur loading.

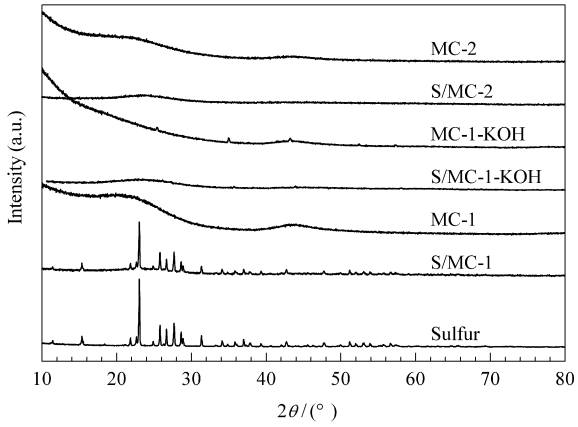

Figure 3. Wide-angle XRD patterns of the sulfur, ordered porous carbons and S/C composites

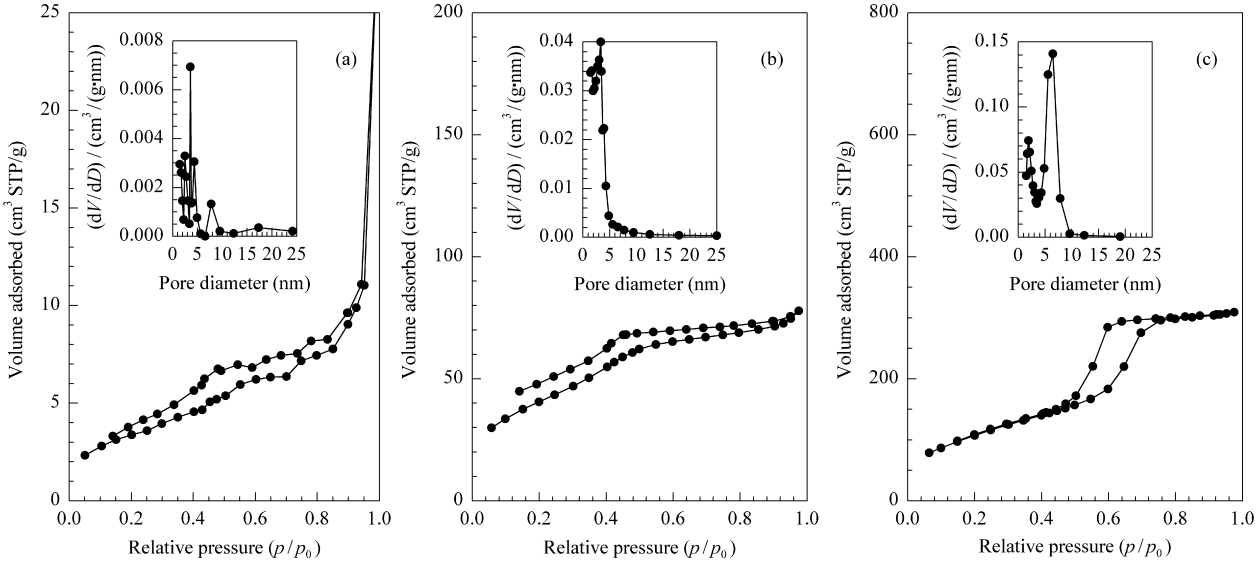

Figure 4. Nitrogen adsorption/desorption isotherms of S/C composites, (a) S/MC-1, (b) S/MC-1-KOH, and (c) S/MC-2 with inset showing their corresponding pore-size distribution

3.3. Electrochemical performance of the sulfur/carbon composites

Figure 5 plots the initial discharge curves of the S/C composite electrodes at a current density of 167.5 mA·g^{-1}. Two typical and obvious voltage plateaus at round 2.3 V and 1.9 V were detected for all the three samples. The upper plateau is related to the reduction of sulfur to polysulfides (Li_2S_x, $4 \leq x \leqslant 8$), and the lower one involves a further reduction of polysulfides to sulfides Li_2S_2 and Li_2S [16,17].

The S/MC-1 composite showed a lower discharge voltage and a smaller specific discharge capacity compared with S/MC-1-KOH and S/MC-2 as shown in Figure 5. The results are probably due to the aggregation of insulating sulfur on the carbon surface thus degrading the electrochemical kinetics of S/MC-1. Besides, an additional voltage plateau appeared at 1.5−1.7 V in S/MC-1, which could be attributed to the lithiation in the carbon frameworks. Both S/MC-1-KOH and S/MC-2 delivered a nearly identical initial specific capacity, around 1200 mAh·g^{-1} (S), indicating the similar utilization of sulfur in the two S/C composites. However, the content of sulfur in S/MC-2 is 58.7% which is much larger than 37.5% for S/MC-1-KOH. Thus, the specific discharge capacity for the S/C composite is 704 mAh·g^{-1} and 450 mAh·g^{-1} for S/MC-2 and S/MC-1-KOH, respectively.

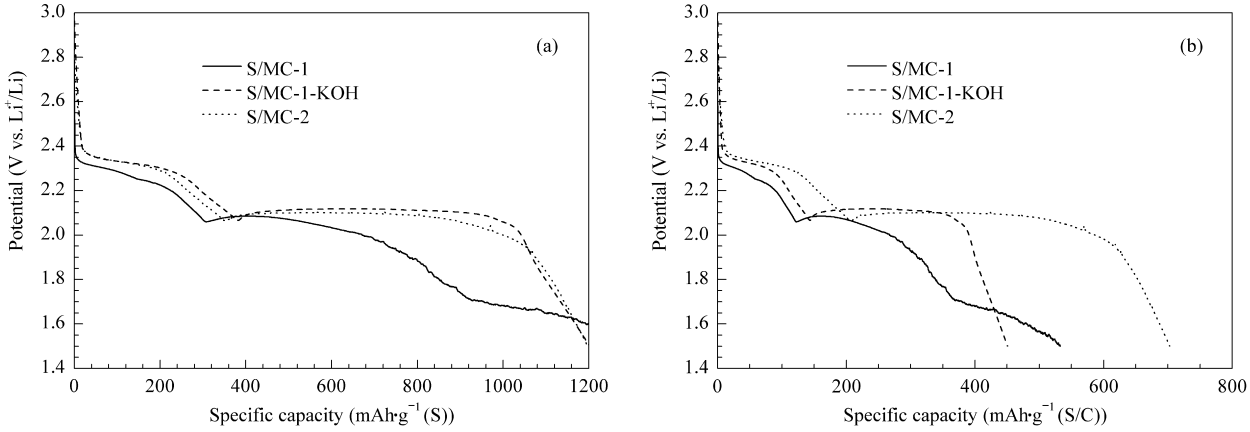

Figure 5. The initial discharge curves of S/C composite electrodes at a current density of 167.5 mA·g^{-1}. Specific capacity was calculated using the mass weight of sulfur (a) and S/C composites (b)

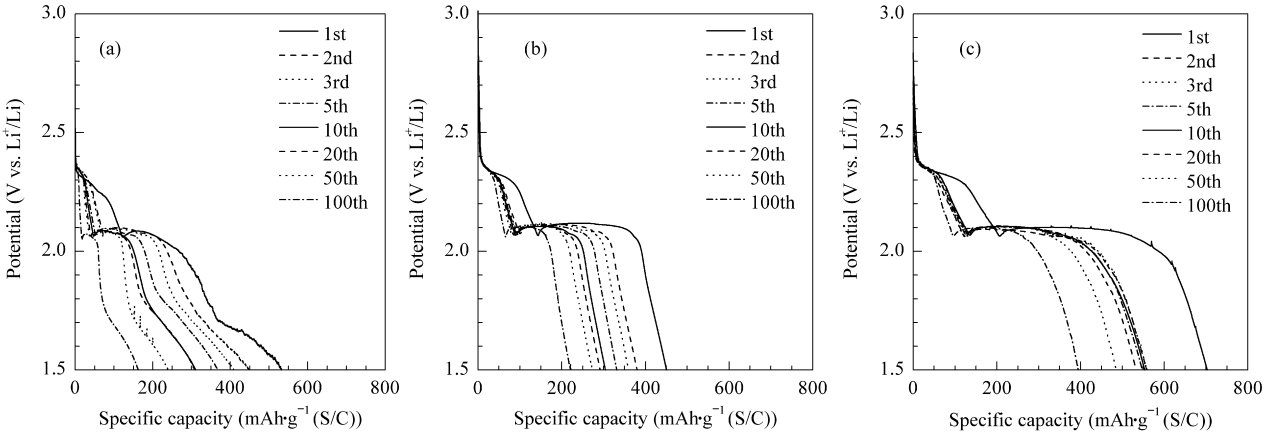

Figure 6. Discharge curves of S/C composite electrodes, (a) S/MC-1, (b) S/MC-1-KOH, and (c) S/MC-2 for different cycles at a current density of 167.5 mA·g^{-1}

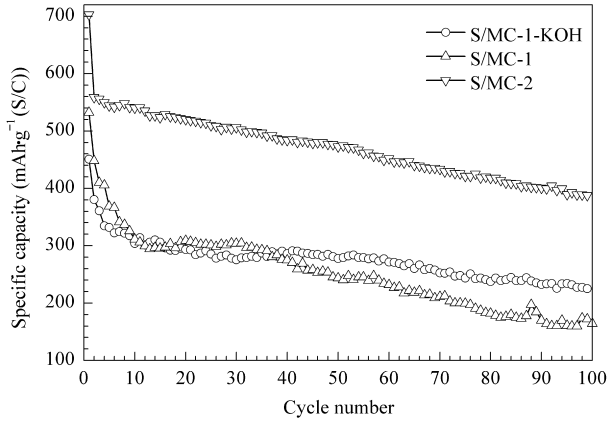

Figure 7. Cycling performances of S/C composite electrodes at a current density of 167.5 mA·g^{-1}

Figure 6 shows the discharge curves of the three S/C composite electrodes for different cycles at a current density of 167.5 mA·g^{-1}. Their specific capacities all decayed as increasing the cycle numbers. The cycling performances of the three S/C composites are shown in Figure 7. The significant decline of the capacity during the first 10 cycles for S/MC-1 and S/MC-1-KOH can be observed. This phenomenon is possibly due to the easy dissolution of polysulfides generated from the sulfur locating at the surface of carbon or in the piled macropores of carbon species. The similar phenomenon has been reported in the other works as well [18,19]. The comparison of cycling performances indicates that S/MC-2 exhibited a superior specific capacity and stability with 55% capacity retention after 100 cycles, followed by S/MC-1-KOH with 50% retention and S/MC-1 with only 33% retention at the same condition.

The different cycling performances are relevant to the sulfur distribution in the three S/C composites. As discussed above, sulfur mainly distributes on the carbon surface in S/MC-1. The un-trapped sulfur could form polysulfides dissolved in the electrolyte solution during the discharge process, which can account for its fast capacity decay. After the KOH activation, the significantly enlarged mesopores (2.9 nm) favored the sulfur encapsulating, which then improved the cycling stability through preventing the polysulfides dissolution. However, the insoluble sulfide Li_2S could segregate and block the inner mesopores, and thus suppress Li_2S oxidation. In addition, the excellent property of S/MC-2 could be attributed to

the unique synergetic effect of its bimodal porous structures [7]. The micropores (1.9 nm) increased the sulfur capacity and the mesopores (6.5 nm) promoted lithium ion mass transport, both of which contributed to the improvement of electrochemical performance and cycling ability.

4. Conclusions

The ordered porous carbon with high surface area and large pore volume were prepared to fabricate the S/C composites for lithium-sulfur battery cathode. The pore structure of the carbon framework was proved to influence the sulfur distribution and thus the electrochemical performance. The bimodal porous S/MC-2 composite delivered a high initial discharge capacity of 704 $mAh \cdot g^{-1}$ (S/C) at a current density of 167.5 $mA \cdot g^{-1}$ with the capacity retention of 55% after 100 cycles. Its superior electrochemical performance can be ascribed to the synergetic effect of its bimodal pore structures. The mesopores in the carbon frame of MC-2 provide channels for molten sulfur diffusion into the micropores and the micropores improved the sulfur encapsulation and depressed the dissolution of polysulfides. Meanwhile, the mesopores in the S/MC-2 composites facilitate the mass transport of Li ion and prevent the block of the pores due to the generation of Li_2S. Design and preparation of porous carbons with desirable structure has been indicated as an effective approach to enhance the sulfur cycle life for high-energy density lithium-sulfur battery.

References

[1] Nelson J, Misra S, YangY, Jackson A, Liu Y J, Wang H L, Dai H J, Andrews J C, Cui Y, Toney M F. *J Am Chem Soc*, 2012, 134(14): 6337
[2] Evers S, Nazar L F. *Acc Chem Res*, 2013, 46(5): 1135
[3] Li G C, Hu J J, Li G R, Ye S H, Gao X P. *J Power Sources*, 2013, 240: 598
[4] Chen S R, Zhai Y P, Xu G L, Jiang Y X, Zhao D Y, Li J T, Huang L, Sun S G. *Electrochimica Acta*, 2011, 56(26): 9549
[5] Wei W, Wang J L, Zhou L J, Yang J, Schumann B, NuLi Y N. *Electrochem Commun*, 2011, 13(5): 399
[6] Deng Z F, Zhang Z A, Lai Y Q, Liu J, Liu Y X, Li J. *Solid State Ionics*, 2013, 238: 44
[7] Liang C D, Dudney N J, Howe J Y. *Chem Mater*, 2009, 21(19): 4724
[8] Meng Y, Gu D, Zhang F Q, Shi Y F, Cheng L, Feng D, Wu Z X, Chen Z X, Wan Y, Stein A, Zhao D Y. *Chem Mater*, 2006, 18(18): 4447
[9] Meng Y, Gu D, Zhang F Q, Shi Y F, Yang H F, Li Z, Yu C Z, Tu B, Zhao D Y. *Angew Chem Int Ed*, 2005, 44(43): 7053
[10] Liu R L, Shi Y F, Wan Y, Meng Y, Zhang F Q, Gu D, Chen Z X, Tu B, Zhao D Y. *J Am Chem Soc*, 2006, 128(35): 11652
[11] Yan Y, Zhang F Q, Meng Y, Tu B, Zhao D Y. *Chem Commun*, 2007, 27: 2867
[12] Xia K S, Gao Q M, Wu C D, Song S Q, Ruan M L. *Carbon*, 2007, 45(10): 1989
[13] Jaroniec M, Kaneko M. *Langmuir*, 1997, 13(24): 6589
[14] Wang J C, Kaskel S. *J Mater Chem*, 2012, 22(45): 23710
[15] Zhou X Y, Xie J, Yang J, Zou Y L, Tang J J, Wang S C, Ma L L, Liao Q C. *J Power Sources*, 2013, 243: 993
[16] Rao M M, Song X Y, Cairns E J. *J Power Sources*, 2012, 205: 474
[17] Xin S, Gu L, Zhao N H, Yin Y X, Zhou L J, Guo Y G, Wan L J. *J Am Chem Soc*, 2012, 134(45): 18510
[18] Wang X F, Fang X P, Guo X W, Wang Z X, Chen L Q. *Electrochimica Acta*, 2013, 97: 238
[19] Yin L C, Wang J L, Lin F J, Yang J, Nuli Y N. *Energy Environ Sci*, 2012, 5(5): 6966